



Alignment and Enhanced Multi-Higgs Production

Subhojit Roy ^{1,*} and Carlos E. M. Wagner ^{1,2,3,4,5,†}

¹*High-Energy Physics Division, Argonne National Laboratory, Argonne, IL 60439, USA*

²*Enrico Fermi Institute, Department of Physics, University of Chicago, Chicago, IL 60637, USA*

³*Kavli Institute for Cosmological Physics, University of Chicago, Chicago, IL 60637, USA*

⁴*Leinweber Center for Theoretical Physics, University of Chicago, Chicago, IL 60637, USA*

⁵*Perimeter Institute for Theoretical Physics, Waterloo, Ontario N2L 2Y5, Canada*

(Dated: May 29, 2026)

Contrary to conventional expectations, we identify a class of extended scalar-sector scenarios in which final states with two, three, or four Higgs bosons constitute the leading discovery channels for new physics at the LHC. In these scenarios, higher-dimensional interactions, together with suppressed Higgs–scalar mixing near the alignment limit, reorganize the decay patterns of new scalar states, suppressing conventional modes while enhancing multi-Higgs final states. We illustrate the emergence of dominant triple- and quadruple-Higgs signatures in two representative realizations: a single-scalar extension of the Standard Model, where higher-dimensional operators suppress conventional two-body decays while preserving couplings to higher-multiplicity Higgs final states; and a two-singlet scenario, where similar signatures arise through cascade decays with a simpler operator structure. In both cases, the new scalar states can be produced via gluon fusion, yielding potentially observable rates for multi-Higgs production at the LHC. Although both realizations lead to identical final states, they exhibit distinct kinematic features reflecting their underlying topologies, providing a direct handle on the dynamics.

I. INTRODUCTION

The discovery of a Higgs boson (h) with mass near 125 GeV [1, 2] completed the particle content of the Standard Model (SM) and initiated a program to directly probe the structure of the scalar sector [3, 4]. A central objective is to uncover the form of the Higgs potential, which remains only indirectly constrained. Current collider strategies focus on Higgs-pair production as the leading probe of the scalar potential, providing direct sensitivity to the Higgs trilinear self-coupling, while higher-multiplicity Higgs final states offer access to quartic interactions. Resonant searches for physics beyond the SM (BSM) further extend this program by targeting new scalar states that can enhance these processes and provide complementary probes of extended scalar sectors. Future collider programs are expected to significantly extend the sensitivity to Higgs self-interactions and to the structure of extended scalar sectors [5–14].

At the LHC, extensive efforts have focused on both resonant and nonresonant di-Higgs production [3, 4, 15–31]. More recently, the experimental program has begun to extend beyond di-Higgs signatures, with dedicated searches for triple-Higgs production, including resonant cascade topologies [32–35]. While these studies already probe part of the relevant signal space, they are not yet guided by a framework in which multi-Higgs final states constitute the dominant collider signatures.

This situation reflects the prevailing theoretical expectation that, in most motivated scenarios, $SU(2)$ symmetry together with the Goldstone Equivalence Theorem relate the Higgs and longitudinal gauge-bosons (W, Z) final states, leading to correlated decay patterns of new

scalar states across the hh , WW , and ZZ channels [36–40]. In particular, mixing between a new scalar and the SM-like Higgs induces couplings to all SM fields, including fermions (f), such that the decay rates of the new scalar into hh , WW , ZZ , and $f\bar{f}$ are controlled primarily by the same mixing angle and are therefore correlated. As a result, di-Higgs signatures are generally accompanied by observable signals in other SM final states. In addition, higher-multiplicity Higgs final states, such as hhh and $hhhh$, are suppressed by phase space and by the structure of scalar interactions, rendering them sub-leading compared to two-body channels. Together, these considerations underpin the standard expectation that the dominant collider manifestations of extended scalar sectors arise in low-multiplicity scalar final states.

These expectations, however, need not hold. Extended scalar sectors (S) can realize regimes in which the decay hierarchy of new scalar states is reorganized, such that higher-multiplicity Higgs final states dominate over conventional two-body decays into SM states. In particular, the partial widths can satisfy

$$\Gamma(S \rightarrow WW, ZZ, \bar{f}f) \ll \Gamma(S \rightarrow hh), \quad (1)$$

or even

$$\Gamma(S \rightarrow hh, WW, ZZ, \bar{f}f) \ll \Gamma(S \rightarrow hhh), \Gamma(S \rightarrow hhhh), \quad (2)$$

leading to scenarios in which multi-Higgs final states become the primary collider signatures. This hierarchy arises from the interplay of alignment and higher-dimensional interactions, where the former suppresses couplings to SM fields, while the latter allows sizable scalar trilinear interactions to persist. Even in the alignment limit, where decays into gauge bosons and fermions

are strongly suppressed, the $S \rightarrow hh$ channel can remain present, but can also be parametrically reduced relative to higher-multiplicity Higgs final states.

In this Letter, we identify a class of scenarios in which resonant multi-Higgs final states emerge as the dominant collider signatures of extended scalar sectors. This behavior can arise through two complementary mechanisms: direct multi-Higgs decays of a single scalar and cascade processes in two-scalar setups [41, 42]. The corresponding collider signatures can be summarized schematically as

$$pp \rightarrow \begin{cases} \text{cascade: } s_1 \rightarrow hs_2 \ (s_2 \rightarrow hh) \rightarrow hhh, \\ \phantom{\text{cascade: }} s_1 \rightarrow s_2s_2 \ (s_2 \rightarrow hh) \rightarrow hhhh, \\ \text{direct: } s \rightarrow hh, hhh, hhhh. \end{cases} \quad (3)$$

Identical final states, hhh and $hhhh$, can arise from structurally distinct underlying dynamics. Despite this, the two mechanisms lead to distinct kinematic features, providing a direct handle for experimental discrimination at colliders. In both realizations, the heavy scalar states (s_1 , s_2 or s) can be produced via gluon fusion, e.g. through vector-like quark (VLQ) loops, while their decays generate the multi-Higgs final states, defining a regime in which hh , hhh and $hhhh$ production provides the leading experimental handle on the underlying dynamics.

This regime contrasts with most previous studies, where enhanced multi-Higgs production is typically accompanied by correlated signatures in gauge boson and fermionic channels [43, 44]. In the scenarios identified here, these conventional decay modes are parametrically suppressed, leaving multi-Higgs final states as the leading probes of the extended scalar sector and motivating a shift in experimental search strategies.

To make these features explicit, we now turn to the underlying framework and its collider implications. We first present the theoretical setup, including both the two-singlet cascade scenario and the one-singlet effective realization, and show how the interplay of alignment and higher-dimensional interactions leads to dominant multi-Higgs final states. We then discuss the collider implications, emphasizing the kinematic structure of the signal and its experimental interpretation. Technical details are discussed in the Appendices.

II. MODEL SETUP AND MECHANISM

A. Two-real singlet scalars extension

We extend the SM by two real gauge-singlet scalars, S_1 and S_2 , and a VLQ $T \sim (3, 1, 2/3)$. After electroweak

symmetry breaking,

$$H = \begin{pmatrix} G^+ \\ \frac{v+h+iG^0}{\sqrt{2}} \end{pmatrix}, \quad S_1 = v_1 + s_1, \quad S_2 = v_2 + s_2, \quad (4)$$

with $v \simeq 246$ GeV. The relevant Lagrangian is

$$\mathcal{L} \supset \frac{1}{2}(\partial_\mu S_1)^2 + \frac{1}{2}(\partial_\mu S_2)^2 - V(H, S_1, S_2) + \bar{T}(i\not{D} - M_T)T - y_{T,1s_1}\bar{T}T - y_{T,2s_2}\bar{T}T. \quad (5)$$

The VLQ induces a loop-generated coupling of the heavier singlet-like state to gluons [45]. In the heavy-fermion limit $M_T \gg m_{s_1}, m_{s_2}$, integrating out T gives

$$\mathcal{L}_{\text{eff}} \supset \frac{\alpha_s}{12\pi} \frac{y_{T,1}}{M_T} s_1 G_{\mu\nu}^a G^{a\mu\nu} + \frac{\alpha_s}{12\pi} \frac{y_{T,2}}{M_T} s_2 G_{\mu\nu}^a G^{a\mu\nu} \quad (6)$$

which enables resonant s_1 and s_2 production through gluon fusion at the LHC. We take $M_T \sim \mathcal{O}(\text{TeV})$, and take Yukawa couplings so that current direct limits can be satisfied while retaining an appreciable production rate. At the renormalizable level, the phenomenologically motivated scalar potential can be parametrized as,

$$\begin{aligned} V_{\text{ren}} = & -\mu_H^2 H^\dagger H + \lambda_H (H^\dagger H)^2 + \frac{m_1^2}{2} S_1^2 + \frac{m_2^2}{2} S_2^2 \\ & + \mu_{12}^2 S_1 S_2 + a_1 S_1 H^\dagger H + a_2 S_2 H^\dagger H \\ & + \kappa S_1 S_2 H^\dagger H + \frac{\lambda_{HS_1}}{2} S_1^2 H^\dagger H + \frac{\lambda_{HS_2}}{2} S_2^2 H^\dagger H \\ & + \frac{\lambda_1}{4} S_1^4 + \frac{\lambda_2}{4} S_2^4 + \frac{\lambda_{12}}{2} S_1^2 S_2^2, \end{aligned} \quad (7)$$

supplemented by the leading higher-dimensional term

$$V_{\text{dim5}} = \frac{c_5}{\Lambda} S_2 (H^\dagger H)^2, \quad (8)$$

where $V(H, S_1, S_2) = V_{\text{ren}} + V_{\text{dim5}}$. We treat this setup as an effective description, without specifying a particular ultraviolet completion. Although other higher-dimensional operators, beyond Eq. (8), may be present, the most important ones for the mechanism under consideration are those which involve a higher power of the portal operator $(H^\dagger H)^n$, $n > 1$, and which affect the mixing of the lightest new scalar with the standard Higgs boson. We focus on the lowest dimensional one, and assume other higher-dimensional operators to lead to subleading effects on the parameter space associated with the mechanism under study.

The higher-dimensional operator, Eq. (8), plays a central role. After symmetry breaking, it contributes differently to the off-diagonal h - s_2 mass-mixing entry and to the cubic $s_2 hh$ interaction. As a result, one can suppress the Higgs admixture of s_2 , approaching the alignment regime at the price of some level of fine-tuning, while keeping its coupling to a Higgs pair sizable. The

essential mechanism is therefore to enhance the double-Higgs decays compared to the conventional decays into fermions and gauge bosons. The scalar mass matrix, vacuum conditions, and alignment relations are collected in Appendix (A) and (B).

The phenomenologically relevant regime is the approximate alignment limit, where the mixings among h and s_1, s_2 are small. This alignment regime is experimentally motivated by Higgs coupling measurements at the LHC, which indicate that the observed 125 GeV Higgs boson is close to the SM-like. In this limit, the couplings of s_1 and s_2 to SM gauge bosons and fermions are suppressed, whereas the scalar cascade interactions can remain unsuppressed. In particular, the trilinear couplings controlling the decays of s_1 are $g_{s_1 s_2 h} = \kappa v$ (see Eq. (B21)) and $g_{s_1 s_2 s_2} = 2\lambda_{12}v_1$ (see Eq. (B22)) so that, depending on kinematics and on the relative sizes of κ and $\lambda_{12}v_1$, either $s_1 \rightarrow hs_2$ or $s_1 \rightarrow s_2 s_2$ can dominate, while all competing SM decay modes remain suppressed in the aligned regime. The VLQ loop-induced decay modes into gg and $\gamma\gamma$ can remain subleading when the scalar cascade couplings, controlled by κ and $\lambda_{12}v_1$, are sufficiently large.

For the lighter state s_2 , the interplay between h - s_2 mass mixing (see Eq. (B5)) and cubic $s_2 hh$ interaction is particularly important. The relevant quantities are

$$M_{hs_2}^2 = v(a_2 + \kappa v_1 + \lambda_{HS_2} v_2) + \frac{c_5}{\Lambda} v^3, \quad (9)$$

$$g_{s_2 hh} = a_2 + \kappa v_1 + \lambda_{HS_2} v_2 + 3 \frac{c_5}{\Lambda} v^2 = \frac{M_{hs_2}^2}{v} + 2 \frac{c_5}{\Lambda} v^2. \quad (10)$$

Both expressions involve the same portal combination ($a_2 + \kappa v_1 + \lambda_{HS_2} v_2$), but differ in c_5 contribution by a factor of three. This mismatch allows a parametric separation between mixing and decay: one can impose $M_{hs_2}^2 \simeq 0$ (alignment) while retaining a sizable trilinear coupling,

$$g_{s_2 hh} \simeq 2 \frac{c_5}{\Lambda} v^2. \quad (11)$$

As a result, s_2 remains highly singlet-like while decaying predominantly into Higgs pairs, with all other two-body decay modes ($ZZ, WW, f\bar{f}$) suppressed. At hadron colliders, s_2 can be produced resonantly via the VLQ-induced effective coupling to gg , as defined in Eq. (6). In contrast to typical resonant di-Higgs scenarios, where decays into WW, ZZ , and $f\bar{f}$ provide correlated search channels [3, 4, 8, 14, 17, 18, 43, 44], here these modes are suppressed by alignment, while the VLQ loop-induced gg and $\gamma\gamma$ channels remain subleading for sufficiently large $s_2 hh$ coupling. Consequently, $s_2 \rightarrow hh$ can dominate with a branching fraction close to 1, making di-Higgs the primary and effectively unique visible probe of s_2 .

We now focus on triple- and quadruple-Higgs production. A similar mechanism, with a tunable s_1 cascade

structure, enables a controlled realization of these final states. As this setup involves some degree of parameter tuning, it is expected to be sensitive to renormalization group (RG) effects. We assume the parameters are evaluated at the relevant scale of the theory. Additional quantum corrections may shift the viable parameter space without altering the qualitative physical picture.

To make these features quantitative, Fig. (1) shows the branching fractions of ϕ_{s_2} (left) and ϕ_{s_1} (center and right) as functions of $\sin\theta_2$, $g_{s_1 s_2 h}$, and $g_{s_1 s_2 s_2}$, respectively, (see Appendix (D) for the computational details of the relevant partial decay widths and branching fractions) for the benchmark $(m_{\phi_{s_1}}, m_{\phi_{s_2}}) = (800, 300)$ GeV, $c_5/\Lambda = 2 \times 10^{-4}$ GeV $^{-1}$ and $c_{g_1} = 3 \times 10^{-6}$ GeV $^{-1}$. For simplicity, in this plot we set the VLQ-induced $s_2 gg$ coupling to zero, as the focus is on triple- and quadruple-Higgs production rather than s_2 production. We have verified, however, that even if it is comparable to c_{g_1} , the qualitative dominance of the $s_2 \rightarrow hh$ decay mode in the low-mixing regime remains unchanged. In the alignment limit the mass eigenstates align with the interaction states, $\phi_{s_1} \simeq s_1$, $\phi_{s_2} \simeq s_2$, and $\phi_h \simeq h$.

The left panel shows $\text{BR}(\phi_{s_2})$ as a function of $\sin\theta_2$. The coupling $g_{s_2 hh}$ and the mixing angle θ_2 are not independent: both are fixed by the off-diagonal mass entry $M_{hs_2}^2 = \frac{1}{2} \sin(2\theta_2) (m_{\phi_h}^2 - m_{\phi_{s_2}}^2)$ and c_5/Λ through Eq. (10). Without loss of generality, we assume that both $\sin 2\theta_2$ and c_5/Λ are positive. Since $m_{\phi_h} < m_{\phi_{s_2}}$, one has $M_{hs_2}^2 < 0$. At exact alignment ($\sin\theta_2 = 0$), $M_{hs_2}^2$ vanishes and $g_{s_2 hh}$ reaches its maximum value $2(c_5/\Lambda)v^2$. As $\sin\theta_2$ increases, $M_{hs_2}^2$ grows in magnitude and, since it is negative, acts against the positive c_5/Λ term in $g_{s_2 hh}$, progressively reducing the overall coupling and, consequently, the di-Higgs branching fraction. Simultaneously, the WW, ZZ , and $b\bar{b}$ decay modes grow as $\sin^2\theta_2$. In the phenomenologically relevant regime $\sin\theta_2 \lesssim 0.01$, one finds $\text{BR}(\phi_{s_2} \rightarrow \phi_h \phi_h) \sim 1$.

The center and right panels show $\text{BR}(\phi_{s_1})$ as functions of $g_{s_1 s_2 h} = \kappa v$ and $g_{s_1 s_2 s_2} = 2\lambda_{12}v_1$, respectively, with $\sin\theta_{1,2} = 0.001$ fixed and the alignment condition $M_{s_1 s_2}^2 = 0$ imposed, corresponding to negligible all pairwise mixings among h, s_1 and s_2 . The small mixing region is chosen to suppress $\phi_{s_1} \rightarrow ZZ, WW, f\bar{f}$ decay modes. At small cubic couplings, the VLQ loop-induced $\phi_{s_1} \rightarrow gg$ mode dominates; as the couplings grow, $\phi_{s_1} \rightarrow \phi_{s_2} \phi_h$ (center) and $\phi_{s_1} \rightarrow \phi_{s_2} \phi_{s_2}$ (right) rapidly take over, with branching fractions approaching unity. Defining the effective branching fractions via the narrow-width approximation, $\text{BR}_{\text{eff}}(hhh) \equiv \text{BR}(\phi_{s_1} \rightarrow \phi_{s_2} \phi_h) \text{BR}(\phi_{s_2} \rightarrow \phi_h \phi_h)$, and $\text{BR}_{\text{eff}}(hhhh) \equiv \text{BR}(\phi_{s_1} \rightarrow \phi_{s_2} \phi_{s_2}) [\text{BR}(\phi_{s_2} \rightarrow \phi_h \phi_h)]^2$, both can approach unity in the appropriate regions of parameter space, establishing triple- and quadruple-Higgs production as the dominant collider signatures in this scenario.

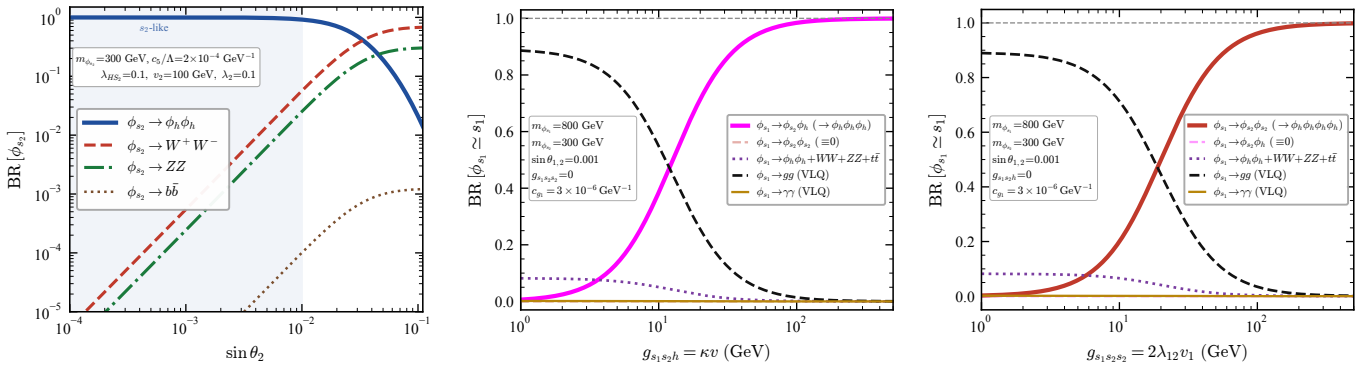


FIG. 1. [Left] Branching ratios of ϕ_{s_2} ($m_{\phi_{s_2}} = 300$ GeV) as a function of the h - s_2 mixing angle $\sin\theta_2$. In the alignment regime ($\sin\theta_2 \lesssim 0.01$, shaded), the mass eigenstates align with the interaction states, and the di-Higgs decay mode dominates over all other channels. [Middle] Branching ratios of ϕ_{s_1} ($m_{\phi_{s_1}} = 800$ GeV) as a function of the cubic coupling $g_{s_1 s_2 h}$, and [Right] $g_{s_1 s_2 s_2}$. In both panels, the condition $M_{s_1 s_2}^2 = 0$ is imposed, and the mixing angles $\sin\theta_1$ and $\sin\theta_2$ are taken to be small, such that $\phi_{s_1} \simeq s_1$, $\phi_{s_2} \simeq s_2$ and $\phi_h \simeq h$. As the cubic couplings increase, the decay channels $s_1 \rightarrow s_2 h$ (middle) and $s_1 \rightarrow s_2 s_2$ (right) become dominant, thereby suppressing the loop-induced VLQ-mediated gg and $\gamma\gamma$ modes. The benchmark parameter choices used for illustration are indicated in each panel.

B. One-real singlet scalar extension

Resonant multi-Higgs final states can also be realized in a minimal extension of the SM with a single real singlet scalar S , supplemented by higher-dimensional operators. We consider the effective scalar potential

$$\begin{aligned}
 V(H, S) = & -\mu_H^2 H^\dagger H + \lambda_H (H^\dagger H)^2 + \frac{m_1^2}{2} S^2 + a_1 S H^\dagger H \\
 & + \frac{\lambda_{HS}}{2} S^2 H^\dagger H + \frac{\lambda_1}{4} S^4 + \frac{c_5}{\Lambda} S (H^\dagger H)^2 \\
 & + \frac{c_7}{\Lambda^3} S (H^\dagger H)^3, \quad (12)
 \end{aligned}$$

with $S = v_s + s$. If one ignores the dimension seven operator, the same mechanism as before can serve to enhance double Higgs production compared to other two-body standard production channels. Moreover, as shown in Appendix (C), the higher-dimensional operators allow one to approach the alignment limit (no mixing between s and h) and suppress the di-Higgs decay $s \rightarrow hh$, while retaining sizable couplings to higher-multiplicity Higgs final states. This is achieved through cancellations among operator contributions, which can make $g_{shh} = 0$ without forcing the $s \rightarrow hhh$ interaction to vanish. In this limit, the coupling takes the form $g_{shhh} = 6 c_7 v^3 / \Lambda^3$, (see Eq. (C8)). As a result, there exist regions of parameter space in which the $s \rightarrow hhh$ decay dominates. While additional higher-dimensional operators, such as $\frac{c_9}{\Lambda^5} S (H^\dagger H)^4$, could, in principle, enhance $s \rightarrow hhhh$ transitions, achieving a regime in which this channel dominates would require highly non-generic parameter choices and correlated cancellations among multiple higher-dimensional operator contributions.

This illustrates a structural difference between the two scenarios: in the minimal singlet extension, suppress-

ing $s \rightarrow hh$ while retaining a sizable $s \rightarrow hhh$ coupling requires a cancellation between Wilson coefficients of operators at different mass dimensions (here c_5 and c_7 , see Eq. (C7)), and dominance of the $s \rightarrow hhhh$ channel would require additional correlated cancellations among still higher-dimensional operators. In the two-singlet cascade scenario, by contrast, multi-Higgs dominance is achieved through alignment conditions of the type familiar from extended Higgs sectors (see, for example, Ref. [46]). Both realizations therefore involve some degree of tuning, but the cascade scenario relies on alignment-type relations rather than on cancellations between operators of different dimensions, and it accommodates both hhh and $hhhh$ final states within the same framework. We therefore focus on the cascade realization in the collider phenomenology.

III. COLLIDER IMPLICATIONS

Having established the regions of parameter space in which multi-Higgs final states dominate, we now turn to the resulting collider signal structure and expected event rates.

Signal structure and normalization.— As established above, the framework admits regions of parameter space in which the effective branching fractions into hh , hhh , and $hhhh$ final states can approach unity. In this regime, multi-Higgs production constitutes the primary collider signature of the extended scalar sector. The observable event rates are therefore controlled predominantly by the production cross section of the parent scalar state. At the LHC, the dominant production mechanism is gluon fusion, induced by heavy colored states or, equivalently, by an effective Xgg interaction [45, 47]. Parametrically,

$\sigma(pp \rightarrow X) \propto \left(\frac{\alpha_s y_T}{12\pi M_T}\right)^2$, and the signal rate is given by $\sigma_{\text{sig}} = \sigma(pp \rightarrow X) \times \text{BR}_{\text{eff}}$. In the region of interest, where $\text{BR}_{\text{eff}} \sim 1$, the multi-Higgs rates are directly set by the production cross section.

As a representative benchmark, we consider a singlet-like scalar with mass $m_{s_1} \simeq 800$ GeV and an effective gluon coupling $c_{g_1} \sim 3 \times 10^{-6}$ GeV $^{-1}$, yielding a production cross section $\sigma(pp \rightarrow X) \sim 15$ fb at leading order using MADGRAPH5_AMC@NLO [48] at $\sqrt{s} = 14$ TeV. For $\text{BR}_{\text{eff}} \sim 1$, this translates into comparable rates for resonant hh , hhh , and $hhhh$ production, corresponding to potentially observable event yields at the LHC.

While di-Higgs production has been extensively studied both theoretically and experimentally, including dedicated searches at the LHC, higher-multiplicity Higgs final states remain comparatively unexplored. In particular, recent experimental efforts have begun to probe triple-Higgs production, including resonant cascade topologies, while searches for four-Higgs final states are still largely absent. Motivated by this emerging experimental direction, and by the distinctive signal structure of the framework, we focus in the following on the collider phenomenology of hhh and $hhhh$ final states arising from cascade decays.

We begin by outlining the characteristic signal topologies and experimental challenges associated with these high-multiplicity final states. In the cascade realization, the heavy state s_1 decays via $s_1 \rightarrow hs_2$ or $s_1 \rightarrow s_2s_2$, followed by $s_2 \rightarrow hh$, leading to hhh and $hhhh$ final states with a characteristic hierarchical resonance structure.

The phenomenologically dominant signatures arise from $h \rightarrow b\bar{b}$, leading to $6b$ and $8b$ final states with large jet multiplicities and nontrivial combinatorial structure.¹ Such final states with high b -jet multiplicities are experimentally challenging due to finite b -tagging efficiency, which suppresses event-level acceptance, as well as large combinatorial ambiguities and overwhelming QCD multijet backgrounds. These challenges are particularly pronounced in the $8b$ channel. Nevertheless, the presence of correlated invariant-mass structures at multiple scales provides powerful handles that can be exploited for signal discrimination.

The dominant background arises from QCD multijet production, with subleading contributions from $t\bar{t}$ -jets. Although these backgrounds can populate high-multiplicity final states and mimic Higgs candidates combinatorially, they are less likely to reproduce the correlated multi-scale resonance structure of the signal.

¹ While we focus on the dominant $h \rightarrow b\bar{b}$ decay mode, subleading channels such as $h \rightarrow \gamma\gamma$ and $h \rightarrow \tau^+\tau^-$ may provide cleaner but lower-rate signatures, and thus offer complementary search channels. In particular, searches exploiting $h \rightarrow \gamma\gamma$ decays have been pursued by the CMS Collaboration in the $4b2\gamma$ final state [34]. For more detail, see the HHH whitepaper [35].

Kinematic structure and topology.— Cascade decays of the form $pp \rightarrow s_1 \rightarrow hs_2$ or $s_1 \rightarrow s_2s_2$, followed by $s_2 \rightarrow hh$, give rise to a hierarchical pattern,

$$b\bar{b} \xleftarrow{m_{b\bar{b}}} h, \quad hh \xleftarrow{m_{hh}} s_2, \quad h^N \xleftarrow{m_{h^N}} s_1, \quad (13)$$

with $N = 3, 4$, leading to correlated invariant-mass scales in the final state.

A key qualitative distinction arises between asymmetric and symmetric cascade topologies. In the asymmetric configuration $pp \rightarrow s_1 \rightarrow hs_2 \rightarrow hhh$, only one Higgs pair originates from the decay of s_2 , leading to a broadened intermediate structure due to combinatorial contamination. In contrast, in the symmetric topology $pp \rightarrow s_1 \rightarrow s_2s_2 \rightarrow hhhh$, the presence of two identical intermediate states introduces correlations that can be exploited to reduce combinatorial ambiguities and improve reconstruction of the intermediate scale.

Topology-driven reconstruction strategies.— The hierarchical structure of the cascade motivates simple reconstruction strategies based on invariant-mass correlations. For an event with N Higgs bosons, we consider all one-to-one assignments of b and \bar{b} jets and select the configuration minimizing

$$\chi_h^2 = \sum_{i=1}^N \frac{\left(m_{b\bar{b}}^{(i)} - m_h\right)^2}{\sigma_h^2}, \quad (14)$$

where σ_h is an analysis-level resolution scale that provides a stable ranking variable for the optimal pairing. This simple χ^2 -based procedure serves as a transparent baseline for Higgs reconstruction, in contrast to more sophisticated approaches based on machine-learning techniques used in experimental analyses [32, 33].

The reconstruction of the intermediate scalar s_2 depends on the topology. In the asymmetric case, combinatorial ambiguity leads to a broadened m_{hh} distribution with a localized signal enhancement. In the symmetric topology, this ambiguity can be reduced by minimizing

$$\Delta_{s_2} = \left| m_{hh}^{(1)} - m_{hh}^{(2)} \right|, \quad (15)$$

with the averaged mass $\bar{m}_{hh} = \frac{m_{hh}^{(1)} + m_{hh}^{(2)}}{2}$ peaking at m_{s_2} .

The heavy scalar s_1 is reconstructed from the full set of Higgs candidates, $m_{h^N}^2 = \left(\sum_{i=1}^N p_{h_i}\right)^2$. These strategies are intended as illustrative benchmarks of the underlying kinematic structure, which can be further exploited in realistic experimental analyses employing multivariate or machine-learning techniques.

Existing constraints and prospects.— Existing LHC searches for triple-Higgs production already provide direct constraints on part of the parameter space. The CMS Collaboration has obtained a 95% CL upper limit of $\sigma(pp \rightarrow hhh \rightarrow 6b) \lesssim 44$ fb [32]. The ATLAS Collaboration has searched for both non-resonant and resonant

triple-Higgs production in the $6b$ final state, explicitly targeting cascade topologies, and reports a 95% CL upper limit of $\sigma(pp \rightarrow hhh) \lesssim 59$ fb [33].

The $hhhh$ channel is even less constrained experimentally. While $pp \rightarrow hhhh \rightarrow 8b$ events could in principle contaminate inclusive triple-Higgs searches through partial reconstruction, such effects are expected to be strongly suppressed. Four-Higgs final states therefore remain largely unexplored and constitute a well-motivated target for dedicated searches.

The benchmark rates considered here remain compatible with current constraints, including those from di-Higgs measurements and searches for additional scalar resonances [3, 4, 15–31, 34, 35]. More generally, the overall signal normalization is controlled by the effective gluon coupling c_{g1} , defined in Eq. (E2). In the absence of a signal, progressively stronger experimental bounds can be accommodated by moving to smaller values of c_{g1} , thereby reducing the production rate while preserving the characteristic multi-Higgs decay topology.

Cascade vs. direct multi-Higgs production.— A qualitatively different behavior arises when multi-Higgs final states originate from direct decays of a single scalar, $s \rightarrow hhh$ or $hhhh$, without intermediate resonances. In this case, invariant-mass combinations probe only a single scale, leading to smoother distributions shaped by phase space. The absence of additional intermediate mass scale implies that reconstruction strategies based on correlated di-Higgs structures are not directly applicable, and dedicated analysis approaches are required.

This distinction provides a direct experimental handle for differentiating between cascade and direct production mechanisms, even when the final states are identical. Additional observables, such as angular separations between b -jets, may provide complementary information. A realistic analysis would combine invariant-mass reconstruction, heavy-flavor tagging, and advanced techniques such as boosted Higgs tagging [49, 50] and multivariate methods [51] to enhance sensitivity.

The scenario identified here also highlights an important difference with previous studies of multi-Higgs production in extended scalar sectors. Enhanced triple-Higgs production in such scenarios has been explored, for instance, in the two-real-singlet model with the asymmetric cascade $pp \rightarrow h_3 \rightarrow h_2 h_1 \rightarrow h_1 h_1 h_1$ [41], as well as in simplified narrow-width approaches emphasizing double-resonant factorization [42]. These studies, which have also motivated recent experimental searches, typically consider regimes where multi-Higgs final states coexist with sizable decays into other SM channels. In contrast, the framework considered here realizes a qualitatively different regime in which hhh and $hhhh$ can become the dominant—and in some cases the only observable signatures over a broad region of parameter space, thereby making resonant multi-Higgs production the primary discovery channel for the underlying scalar dynamics.

IV. CONCLUSIONS

We have identified a class of scenarios in which multi-Higgs final states, in particular double-, triple- and quadruple-Higgs channels, can become the dominant collider signatures of extended scalar sectors. Contrary to the conventional expectation that higher-multiplicity Higgs production is strongly suppressed, the decay structure of heavy scalar states can be reorganized such that hh , hhh and $hhhh$ production is enhanced, while conventional SM decay modes and lower-multiplicity Higgs channels are parametrically suppressed. In this regime, multi-Higgs final states can provide the primary and, in some cases essentially unique, probes of the extended scalar sector, with potentially sizable production rates at the LHC.

This behavior can be realized through the interplay of alignment and enhanced scalar interactions, including higher-dimensional operators, which suppress competing decay channels while preserving sizable couplings responsible for multi-Higgs production. As a result, both cascade and direct multi-Higgs production can occur with effective branching fractions approaching close to unity.

Identical hhh and $hhhh$ final states can originate from distinct mechanisms with qualitatively different kinematic structures. Cascade topologies generate correlated invariant-mass features associated with intermediate resonances, whereas direct production yields smooth distributions governed by phase space alone, with no intermediate resonant structure imprinted on the final state. These features can be systematically exploited through an event-level hierarchical reconstruction strategy, allowing the underlying decay pattern to be resolved and the origin of the signal to be identified.

Taken together, these results establish triple- and quadruple-Higgs production as key probes of extended scalar sectors, beyond the standard di-boson searches. In the regions identified here, where conventional search channels are suppressed, such multi-Higgs signatures can become the primary, and in some cases essentially unique, discovery modes for new scalar dynamics at the LHC and future colliders.

Acknowledgments. We thank Tim Hobbs, Keisuke Harigaya, Young-Kee Kim, Peiran Li, Zhen Liu, Lian-Tao Wang and the ATLAS group of the University of Chicago for various insightful discussions. SR is supported by the U.S. Department of Energy under contracts No. DEAC02-06CH11357 at the Argonne National Laboratory. SR would like to thank the University of Chicago, Fermilab and Perimeter Institute where a significant part of this work was carried out. The work of CW at the University of Chicago has been supported by the DOE grant DE-SC0013642.

Note added: While this work was being completed, Ref. [52] appeared, which also explores the role of higher-

dimensional Higgs operators in enhancing Higgs-rich final states of heavy resonances. In contrast, we focus on a complementary regime in which conventional decay modes are suppressed, for instance due to alignment, so that multi-Higgs final states can become the dominant collider signatures of the extended scalar sectors.

Appendix A: Vacuum structure and tadpole equations

The full scalar potential is

$$V(H, S_1, S_2) = V_{\text{ren}} + \frac{c_5}{\Lambda} S_2 (H^\dagger H)^2, \quad (\text{A1})$$

where V_{ren} is given in Eq. (7). Evaluating the potential at the classical background values yields

$$\begin{aligned} V_0 = & -\frac{1}{2}\mu_H^2 v^2 + \frac{1}{4}\lambda_H v^4 + \frac{1}{2}m_1^2 v_1^2 + \frac{1}{2}m_2^2 v_2^2 + \mu_{12}^2 v_1 v_2 \\ & + \frac{1}{2}a_1 v_1 v^2 + \frac{1}{2}a_2 v_2 v^2 + \frac{1}{2}\kappa v_1 v_2 v^2 + \frac{1}{4}\lambda_{HS_1} v_1^2 v^2 \\ & + \frac{1}{4}\lambda_{HS_2} v_2^2 v^2 + \frac{1}{4}\lambda_1 v_1^4 + \frac{1}{4}\lambda_2 v_2^4 + \frac{1}{2}\lambda_{12} v_1^2 v_2^2 + \frac{c_5}{4\Lambda} v_2 v^4. \end{aligned} \quad (\text{A2})$$

The vacuum conditions follow from

$$\frac{\partial V_0}{\partial v} = 0, \quad \frac{\partial V_0}{\partial v_1} = 0, \quad \frac{\partial V_0}{\partial v_2} = 0. \quad (\text{A3})$$

Explicitly,

$$\begin{aligned} 0 = & -\mu_H^2 + \lambda_H v^2 + a_1 v_1 + a_2 v_2 + \kappa v_1 v_2 + \frac{1}{2}\lambda_{HS_1} v_1^2 \\ & + \frac{1}{2}\lambda_{HS_2} v_2^2 + \frac{c_5}{\Lambda} v^2 v_2, \end{aligned} \quad (\text{A4})$$

$$\begin{aligned} 0 = & m_1^2 v_1 + \mu_{12}^2 v_2 + \frac{1}{2}a_1 v^2 + \frac{1}{2}\kappa v^2 v_2 + \frac{1}{2}\lambda_{HS_1} v_1 v^2 \\ & + \lambda_1 v_1^3 + \lambda_{12} v_1 v_2^2, \end{aligned} \quad (\text{A5})$$

$$\begin{aligned} 0 = & m_2^2 v_2 + \mu_{12}^2 v_1 + \frac{1}{2}a_2 v^2 + \frac{1}{2}\kappa v^2 v_1 + \frac{1}{2}\lambda_{HS_2} v_2 v^2 \\ & + \lambda_2 v_2^3 + \lambda_{12} v_1^2 v_2 + \frac{c_5}{4\Lambda} v^4. \end{aligned} \quad (\text{A6})$$

A convenient way to solve these equations is to trade the mass parameters μ_H^2, m_1^2, m_2^2 for the vacuum expectation values and couplings.

Appendix B: Scalar mass matrix, alignment, and cubic couplings

The full scalar potential is

$$V(H, S_1, S_2) = V_{\text{ren}} + \frac{c_5}{\Lambda} S_2 (H^\dagger H)^2, \quad (\text{B1})$$

where V_{ren} is given in Eq. (7). In the (h, s_1, s_2) basis, the CP -even mass-squared matrix is

$$\mathcal{M}_{ij}^2 = \left. \frac{\partial^2 V}{\partial \varphi_i \partial \varphi_j} \right|_{\text{vev}}, \quad \varphi_i = (h, s_1, s_2). \quad (\text{B2})$$

Using the tadpole relations, the entries are

$$M_{hh}^2 = 2\lambda_H v^2 + \frac{2c_5}{\Lambda} v^2 v_2, \quad (\text{B3})$$

$$M_{hs_1}^2 = v(a_1 + \kappa v_2 + \lambda_{HS_1} v_1), \quad (\text{B4})$$

$$M_{hs_2}^2 = v(a_2 + \kappa v_1 + \lambda_{HS_2} v_2) + \frac{c_5}{\Lambda} v^3, \quad (\text{B5})$$

$$M_{s_1 s_1}^2 = m_1^2 + \frac{1}{2}\lambda_{HS_1} v^2 + 3\lambda_1 v_1^2 + \lambda_{12} v_2^2, \quad (\text{B6})$$

$$M_{s_2 s_2}^2 = m_2^2 + \frac{1}{2}\lambda_{HS_2} v^2 + 3\lambda_2 v_2^2 + \lambda_{12} v_1^2, \quad (\text{B7})$$

$$M_{s_1 s_2}^2 = \mu_{12}^2 + \frac{1}{2}\kappa v^2 + 2\lambda_{12} v_1 v_2. \quad (\text{B8})$$

The physical mass eigenstates are obtained via an orthogonal rotation,

$$\begin{pmatrix} h \\ s_1 \\ s_2 \end{pmatrix} = R \begin{pmatrix} \phi_h \\ \phi_{s_1} \\ \phi_{s_2} \end{pmatrix}, \quad (\text{B9})$$

where ϕ_h is identified with the observed 125 GeV Higgs boson, while ϕ_{s_1} and ϕ_{s_2} denote the heavier and lighter singlet-like mass eigenstates with masses m_{s_1} and m_{s_2} , respectively. In the small-mixing limit, the eigenstates align with the interaction basis, $\phi_h \simeq h$, $\phi_{s_1} \simeq s_1$, and $\phi_{s_2} \simeq s_2$, whereas for larger mixing all three states contain admixtures of h , s_1 , and s_2 .

In the phenomenologically relevant regime considered here, we impose the condition $M_{s_1 s_2}^2 = 0$ for simplicity of the discussion. Although this condition is not necessary for the scenario under consideration, it removes the direct off-diagonal entry between s_1 and s_2 in the interaction basis, thereby simplifying the analysis. We emphasize, however, that in the full 3×3 system this condition alone does not eliminate all s_1 - s_2 mixing: even with $M_{s_1 s_2}^2 = 0$, the states s_1 and s_2 can mix indirectly through their common coupling to h via the entries $M_{hs_1}^2$ and $M_{hs_2}^2$. In the limit where all off-diagonal entries are small compared to the relevant diagonal mass splittings, as specified below, the mixing angles are perturbatively small and the rotation matrix R can be expanded accordingly. To leading order in this small-mixing expansion, the dominant mixing angles θ_1 and θ_2 , parametrizing the h - s_1 and h - s_2 mixings respectively, are given by

$$\tan 2\theta_1 \simeq \frac{2M_{hs_1}^2}{M_{s_1 s_1}^2 - M_{hh}^2}, \quad (\text{B10})$$

$$\tan 2\theta_2 \simeq \frac{2M_{hs_2}^2}{M_{s_2 s_2}^2 - M_{hh}^2}. \quad (\text{B11})$$

The residual s_1 - s_2 mixing, even with $M_{s_1 s_2}^2 = 0$, arises at higher order from the two-step path $s_1 \rightarrow h \rightarrow s_2$, and is parametrically of $\mathcal{O}(\theta_1 \theta_2)$. In the aligned regime this contribution is doubly suppressed and can be neglected at leading order, justifying the use of θ_1 and θ_2 as the effective parameters controlling the mixing structure [46].

The aligned regime relevant for our phenomenology is characterized by

$$|M_{hs_1}^2| \ll |M_{s_1s_1}^2 - M_{hh}^2|, \quad |M_{hs_2}^2| \ll |M_{s_2s_2}^2 - M_{hh}^2|, \quad (\text{B12})$$

. This suggests the approximate alignment conditions

$$a_1 + \kappa v_2 + \lambda_{HS_1} v_1 \simeq 0, \quad (\text{B13})$$

$$a_2 + \kappa v_1 + \lambda_{HS_2} v_2 + \frac{c_5}{\Lambda} v^2 \simeq 0. \quad (\text{B14})$$

These relations keep the Higgs-like state close to the SM direction while leaving the cubic scalar couplings sufficiently flexible to generate dominant cascade decays. As emphasized before, for simplicity of the analysis, we also impose the condition

$$|M_{s_1s_2}^2| \ll |M_{s_1s_1}^2 - M_{s_2s_2}^2| \quad (\text{B15})$$

which leads to

$$\mu_{12}^2 + \frac{1}{2} \kappa v^2 + 2\lambda_{12} v_1 v_2 \simeq 0. \quad (\text{B16})$$

The cascade-decay structure in the parameter region of interest is governed by the scalar trilinear interactions

$$s_1 \rightarrow h s_2, \quad s_1 \rightarrow s_2 s_2, \quad s_2 \rightarrow h h, \quad (\text{B17})$$

controlled respectively by the couplings $g_{s_1 s_2 h}$, $g_{s_1 s_2 s_2}$, and $g_{s_2 h h}$. The relevant interactions are defined through

$$\begin{aligned} \mathcal{L}_{\text{int}} \supset & -\frac{1}{2} g_{s_1 h h} s_1 h^2 - \frac{1}{2} g_{s_2 h h} s_2 h^2 - g_{s_1 s_2 h} s_1 s_2 h \\ & - \frac{1}{2} g_{s_1 s_2 s_2} s_1 s_2^2. \end{aligned} \quad (\text{B18})$$

Expanding the potential yields

$$g_{s_1 h h} = a_1 + \kappa v_2 + \lambda_{HS_1} v_1, \quad (\text{B19})$$

$$g_{s_2 h h} = a_2 + \kappa v_1 + \lambda_{HS_2} v_2 + 3 \frac{c_5}{\Lambda} v^2, \quad (\text{B20})$$

$$g_{s_1 s_2 h} = \kappa v, \quad (\text{B21})$$

$$g_{s_1 s_2 s_2} = 2\lambda_{12} v_1. \quad (\text{B22})$$

In the alignment limit, using Eq. (B13), one finds that

$$g_{s_1 h h} \simeq 0. \quad (\text{B23})$$

The important structural point is that the combination controlling $g_{s_2 h h}$ is not identical to the one controlling the h - s_2 mass mixing in Eq. (B5). It is therefore possible to suppress the Higgs admixture of s_2 while keeping the cubic coupling to a Higgs pair sizable. Using the alignment relation in Eq. (B14), one obtains

$$g_{s_2 h h} \simeq 2 \frac{c_5}{\Lambda} v^2. \quad (\text{B24})$$

This is the central mechanism underlying the dominance of $s_2 \rightarrow h h$ in our setup.

Appendix C: One-singlet extension scenario for dominant multi-Higgs decays

The phenomenologically motivated potential is expressed in Eq. (12). The CP -even mass-squared matrix in the (h, s) basis contains the off-diagonal entry

$$M_{hs}^2 = v \left(a_1 + \lambda_{HS} v_s + \frac{c_5}{\Lambda} v^2 + \frac{3c_7}{4\Lambda^3} v^4 \right). \quad (\text{C1})$$

Exact alignment is obtained by imposing $M_{hs}^2 = 0$, which fixes

$$a_1 = -\lambda_{HS} v_s - \frac{c_5}{\Lambda} v^2 - \frac{3c_7}{4\Lambda^3} v^4. \quad (\text{C2})$$

The interactions relevant for resonant multi-Higgs decays are

$$g_{shh} = a_1 + \lambda_{HS} v_s + \frac{3c_5}{\Lambda} v^2 + \frac{15c_7}{4\Lambda^3} v^4, \quad (\text{C3})$$

$$g_{shhh} = \frac{3}{\Lambda^3} (5c_7 v^3 + 2c_5 v \Lambda^2). \quad (\text{C4})$$

After imposing the alignment condition in Eq. (C2), these become

$$g_{shh}^{\text{align}} = \frac{1}{\Lambda^3} (3c_7 v^4 + 2c_5 v^2 \Lambda^2), \quad (\text{C5})$$

$$g_{shhh}^{\text{align}} = \frac{3}{\Lambda^3} (5c_7 v^3 + 2c_5 v \Lambda^2). \quad (\text{C6})$$

This shows explicitly that alignment alone does not suppress the di-Higgs channel: even for vanishing h - s mixing, g_{shh} remains nonzero in general. Now, suppressing the di-Higgs channel therefore requires an additional condition beyond alignment,

$$g_{shh}^{\text{align}} = 0.$$

Solving this for c_5 gives

$$c_5 = -\frac{3c_7 v^2}{2\Lambda^2}. \quad (\text{C7})$$

After this substitution, g_{shhh} reduces to

$$g_{shhh} = \frac{6c_7 v^3}{\Lambda^3}. \quad (\text{C8})$$

Therefore, the cancellation of the di-Higgs coupling does not force the $s \rightarrow h h h$ interaction to vanish.

In principle, extending the EFT with higher-dimensional operators such as $\frac{c_9}{\Lambda^5} S(H^\dagger H)^4$ can generate $s \rightarrow h h h h$ interactions. However, realizing a regime in which both g_{shh} and g_{shhh} are suppressed while g_{shhhh} remains sizable (for example, one finds $g_{shhhh} = 24 c_9 v^4 / \Lambda^5$ in this limit) requires highly correlated relations among multiple operator coefficients, and is therefore non-generic. For this reason, while the EFT formally allows the construction of higher-multiplicity Higgs final states in the minimal singlet scenario, their realization relies on nontrivial cancellations. In contrast, the two-singlet cascade scenario discussed in the main text achieves multi-Higgs dominance in a relatively more natural and robust manner.

Appendix D: Partial decay widths

This appendix collects the partial-width formulas used to produce Fig. (1). The two-body phase-space momentum for a decay $M \rightarrow m_1 + m_2$ is

$$p_{\text{cm}}(M; m_1, m_2) = \frac{\sqrt{\lambda(M^2, m_1^2, m_2^2)}}{2M}, \quad (\text{D1})$$

where $\lambda(a, b, c) = a^2 + b^2 + c^2 - 2ab - 2bc - 2ca$ is the Källén function, with the threshold condition $M \geq m_1 + m_2$.

The di-Higgs decay rate of ϕ_{s_2} depends on the physical $\phi_{s_2}\phi_h\phi_h$ coupling, G_{eff} , which is obtained by expressing the interaction-basis fields in terms of the mass eigenstates via the rotation R of Eq. (B9) and extracting the coefficient of the $\phi_{s_2}\phi_h^2$ operator. In the limit $\theta_1, \theta_{s_1 s_2} \rightarrow 0$, the $\phi_{s_2}\phi_h\phi_h$ vertex receives contributions only from the h - s_2 mixing sector, and the rotation R effectively reduces to a 2×2 rotation in the (h, s_2) subspace parametrized by θ_2 alone. Including all four cubic interactions of the scalar potential, one finds

$$G_{\text{eff}} = g_{s_2 h h} c_{\theta_2} (1 - 3s_{\theta_2}^2) + g_{h h h} s_{\theta_2} c_{\theta_2}^2 + g_{h s_2 s_2} s_{\theta_2} (s_{\theta_2}^2 - 2c_{\theta_2}^2) + g_{s_2 s_2 s_2} s_{\theta_2}^2 c_{\theta_2} \quad (\text{D2})$$

where $c_{\theta_2} \equiv \cos \theta_2$, $s_{\theta_2} \equiv \sin \theta_2$. The partial width is

$$\Gamma(\phi_{s_2} \rightarrow \phi_h \phi_h) = \frac{G_{\text{eff}}^2 p_{\text{cm}}(m_{\phi_{s_2}}; m_{\phi_h}, m_{\phi_h})}{16\pi m_{\phi_{s_2}}^2}. \quad (\text{D3})$$

In the alignment limit ($\sin \theta_2 \rightarrow 0$), $G_{\text{eff}} \rightarrow g_{s_2 h h} \simeq 2(c_5/\Lambda)v^2$, as found in Eq. (B24).

The decay modes of ϕ_{s_2} into various SM particles are controlled by its doublet admixture, $\sin \theta_2$, and are therefore universally suppressed by $\sin^2 \theta_2$. The corresponding partial widths are given by

$$\Gamma(\phi_{s_2} \rightarrow W^+ W^-) = \frac{\sin^2 \theta_2 G_F m_{\phi_{s_2}}^3}{8\pi\sqrt{2}} (1 - 4x_W + 12x_W^2) \times \sqrt{1 - 4x_W}, \quad (\text{D4})$$

$$\Gamma(\phi_{s_2} \rightarrow Z Z) = \frac{\sin^2 \theta_2 G_F m_{\phi_{s_2}}^3}{16\pi\sqrt{2}} (1 - 4x_Z + 12x_Z^2) \times \sqrt{1 - 4x_Z}, \quad (\text{D5})$$

$$\Gamma(\phi_{s_2} \rightarrow f \bar{f}) = \frac{N_c \sin^2 \theta_2 (m_f/v)^2 m_{\phi_{s_2}}}{8\pi} \left(1 - \frac{4m_f^2}{m_{\phi_{s_2}}^2}\right)^{3/2} \quad (\text{D6})$$

where $x_{W,Z} \equiv (m_{W,Z}/m_{\phi_{s_2}})^2$ and $N_c = 3(1)$ for quarks (leptons). In the alignment limit $\sin \theta_2 \rightarrow 0$, the direct coupling of ϕ_{s_2} to SM gauge bosons and fermions vanishes, while the trilinear coupling $\phi_{s_2}\phi_h\phi_h$ can remain nonzero. Consequently, in the framework considered here, the decay modes into SM gauge bosons and

fermions are suppressed by alignment, while $\text{BR}(\phi_{s_2} \rightarrow \phi_h \phi_h) \rightarrow 1$.

In the alignment limit, $\phi_{s_1} \rightarrow \phi_{s_2}\phi_h$ and $\phi_{s_1} \rightarrow \phi_{s_2}\phi_{s_2}$ decay processes are mostly controlled by the cubic terms $g_{s_1 s_2 h} = \kappa v$ and $g_{s_1 s_2 s_2} = 2\lambda_{12}v_1$, corrections from the full rotation matrix R enter at $\mathcal{O}(\sin^2 \theta_{1,2})$ and are negligible for $\sin \theta_{1,2} \lesssim 0.001$. In this limit, the partial widths for the two cascade channels are

$$\Gamma(\phi_{s_1} \rightarrow \phi_{s_2}\phi_h) \simeq \frac{g_{s_1 s_2 h}^2 p_{\text{cm}}(m_{\phi_{s_1}}; m_{\phi_{s_2}}, m_{\phi_h})}{8\pi m_{\phi_{s_1}}^2}, \quad (\text{D7})$$

$$\Gamma(\phi_{s_1} \rightarrow \phi_{s_2}\phi_{s_2}) \simeq \frac{g_{s_1 s_2 s_2}^2 p_{\text{cm}}(m_{\phi_{s_1}}; m_{\phi_{s_2}}, m_{\phi_{s_2}})}{16\pi m_{\phi_{s_1}}^2}. \quad (\text{D8})$$

The decay modes of ϕ_{s_1} into WW , ZZ , and $f\bar{f}$ are analogous to those in Eqs. (D4), (D5), and (D6), with the replacements $\sin \theta_2 \rightarrow \sin \theta_1$ and $m_{\phi_{s_2}} \rightarrow m_{\phi_{s_1}}$. The VLQ loop-induced widths $\Gamma(\phi_{s_1} \rightarrow gg)$ and $\Gamma(\phi_{s_1} \rightarrow \gamma\gamma)$ are given in Eqs. (E7) and (E8).

Appendix E: VLQ-induced gluon coupling

The VLQ induces the effective interaction

$$\mathcal{L}_{\text{eff}} \supset c_{g1} s_1 G_{\mu\nu}^a G^{a\mu\nu}, \quad (\text{E1})$$

with

$$c_{g1} = \frac{\alpha_s}{16\pi} \frac{y_{T,1}}{M_T} A_{1/2}(\tau_T), \quad \tau_T = \frac{4M_T^2}{m_{s_1}^2}. \quad (\text{E2})$$

The standard spin-1/2 loop function is

$$A_{1/2}(\tau) = 2\tau [1 + (1 - \tau)f(\tau)], \quad (\text{E3})$$

where

$$f(\tau) = \begin{cases} \arcsin^2(\tau^{-1/2}), & \tau \geq 1, \\ -\frac{1}{4} \left[\ln \left(\frac{1 + \sqrt{1 - \tau}}{1 - \sqrt{1 - \tau}} \right) - i\pi \right]^2, & \tau < 1. \end{cases} \quad (\text{E4})$$

In the heavy-fermion limit,

$$A_{1/2}(\tau) \rightarrow \frac{4}{3}, \quad (\text{E5})$$

and combining Eqs. (E1) and (E2), one recovers the form given in Eq. (6). Thus, the resonant production cross section scales parametrically as

$$\sigma(pp \rightarrow s_1) \propto \left| \frac{y_{T,1}}{M_T} A_{1/2}(\tau_T) \right|^2. \quad (\text{E6})$$

Current LHC searches push top-like vector-like quarks into the TeV range, with pair-production limits typically excluding masses around 1.4–1.6 TeV and single-production searches constraining the corresponding electroweak mixing parameters for masses up to about 2 TeV,

depending on the assumed couplings and branching fractions [53–56]. In the present work we therefore treat c_{g1} as an effective low-energy parameter generated by integrating out a heavy VLQ. For the benchmark value $c_{g1} \sim 3 \times 10^{-6} \text{ GeV}^{-1}$, the heavy-fermion expression in Eq. (E2) implies M_T in the TeV range for the Yukawa coupling $y_{T,1} \sim 1$. This remains compatible with a perturbative effective description and should be viewed as an illustrative benchmark rather than a complete UV fit to current direct-search limits.

The VLQ effective operators induce decays which are given by,

$$\Gamma(s_1 \rightarrow gg) = \frac{2c_{g1}^2 m_{s1}^3}{\pi}, \quad (\text{E7})$$

$$\Gamma(s_1 \rightarrow \gamma\gamma) = \frac{c_\gamma^2 m_{s1}^3}{4\pi}, \quad c_\gamma = 2\frac{\alpha}{\alpha_s} Q_T^2 N_c c_{g1}. \quad (\text{E8})$$

The corresponding expressions for the s_2 interactions follow from the replacements $m_{s1} \rightarrow m_{s2}$ and $y_{T,1} \rightarrow y_{T,2}$ in the above relations.

* sroy@anl.gov

† cwagner@uchicago.edu

- [1] G. Aad *et al.* (ATLAS), *Phys. Lett. B* **716**, 1 (2012), arXiv:1207.7214 [hep-ex].
- [2] S. Chatrchyan *et al.* (CMS), *Phys. Lett. B* **716**, 30 (2012), arXiv:1207.7235 [hep-ex].
- [3] M. Cepeda *et al.*, CERN Yellow Rep. Monogr. **7**, 221 (2019), arXiv:1902.00134 [hep-ph].
- [4] J. Alison *et al.*, *Rev. Phys.* **5**, 100045 (2020), arXiv:1910.00012 [hep-ph].
- [5] H. Al Ali *et al.*, *Rept. Prog. Phys.* **85**, 084201 (2022), arXiv:2103.14043 [hep-ph].
- [6] J. de Blas, J. Gu, and Z. Liu, *Phys. Rev. D* **106**, 073007 (2022), arXiv:2203.04324 [hep-ph].
- [7] M. Forsslund and P. Meade, *JHEP* **01**, 182 (2024), arXiv:2308.02633 [hep-ph].
- [8] S. Di Vita, G. Durieux, C. Grojean, J. Gu, Z. Liu, G. Panico, M. Riembau, and T. Vantalon, *JHEP* **02**, 178 (2018), arXiv:1711.03978 [hep-ph].
- [9] J. Tian and K. Fujii (ILD), *PoS EPS-HEP2013*, 316 (2013), arXiv:1311.6528 [hep-ph].
- [10] T. Barklow, K. Fujii, S. Jung, R. Karl, J. List, T. Ogawa, M. E. Peskin, and J. Tian, *Phys. Rev. D* **97**, 053003 (2018), arXiv:1708.08912 [hep-ph].
- [11] D. d’Enterria, *PoS ICHEP2016*, 434 (2017), arXiv:1701.02663 [hep-ex].
- [12] M. Forsslund and P. Meade, *JHEP* **08**, 185 (2022), arXiv:2203.09425 [hep-ph].
- [13] P. Li, Z. Liu, and K.-F. Lyu, *Phys. Rev. D* **109**, 073009 (2024), arXiv:2401.08756 [hep-ph].
- [14] F. Maltoni, G. Ventura, and E. Vryonidou, *JHEP* **12**, 183 (2024), arXiv:2406.06670 [hep-ph].
- [15] G. Aad *et al.* (ATLAS), *Phys. Rev. Lett.* **133**, 101801 (2024), arXiv:2406.09971 [hep-ex].
- [16] A. Tumasyan *et al.* (CMS), *Phys. Rev. Lett.* **129**, 081802 (2022), arXiv:2202.09617 [hep-ex].
- [17] G. Aad *et al.* (ATLAS), *Phys. Rev. Lett.* **132**, 231801 (2024), arXiv:2311.15956 [hep-ex].
- [18] A. Hayrapetyan *et al.* (CMS), *Phys. Rept.* **1115**, 368 (2025), arXiv:2403.16926 [hep-ex].
- [19] A. Tumasyan *et al.* (CMS), *Phys. Rev. Lett.* **131**, 041803 (2023), arXiv:2205.06667 [hep-ex].
- [20] A. M. Sirunyan *et al.* (CMS), *JHEP* **03**, 257 (2021), arXiv:2011.12373 [hep-ex].
- [21] G. Aad *et al.* (CMS, ATLAS), (2026), arXiv:2602.23991 [hep-ex].
- [22] C. Collaboration (CMS), *Projection of CMS experimental reach on HH production at HL-LHC*, Tech. Rep. (CERN, Geneva, 2025).
- [23] A. Tumasyan *et al.* (CMS), *JHEP* **02**, 040 (2025), arXiv:2407.13872 [hep-ex].
- [24] G. Aad *et al.* (ATLAS), *Phys. Lett. B* **800**, 135103 (2020), arXiv:1906.02025 [hep-ex].
- [25] G. Aad *et al.* (ATLAS), *JHEP* **07**, 040 (2023), arXiv:2209.10910 [hep-ex].
- [26] M. Aaboud *et al.* (ATLAS), *Phys. Rev. Lett.* **121**, 191801 (2018), [Erratum: *Phys.Rev.Lett.* **122**, 089901 (2019)], arXiv:1808.00336 [hep-ex].
- [27] G. Aad *et al.* (ATLAS), *Phys. Rev. D* **105**, 092002 (2022), arXiv:2202.07288 [hep-ex].
- [28] G. Aad *et al.* (ATLAS), *Phys. Rev. D* **106**, 052001 (2022), arXiv:2112.11876 [hep-ex].
- [29] G. Aad *et al.* (ATLAS, CMS), (2025), arXiv:2504.00672 [hep-ex].
- [30] A. Hayrapetyan *et al.* (CMS), *JHEP* **12**, 178 (2025), arXiv:2508.11494 [hep-ex].
- [31] A. M. Sirunyan *et al.* (CMS), *JHEP* **01**, 054 (2018), arXiv:1708.04188 [hep-ex].
- [32] CMS Collaboration, *Search for nonresonant triple Higgs boson production in the six b-quark final state in proton-proton collisions at 13 TeV*, Tech. Rep. CMS-PAS-HIG-24-012 (CERN, 2025).
- [33] G. Aad *et al.* (ATLAS), *Phys. Rev. D* **111**, 032006 (2025), arXiv:2411.02040 [hep-ex].
- [34] *Search for triple Higgs production in Run2 data of CMS using 4b2gamma final state.*, Tech. Rep. (CERN, Geneva, 2025).
- [35] H. Abouabid *et al.*, *Eur. Phys. J. C* **84**, 1183 (2024), arXiv:2407.03015 [hep-ph].
- [36] J. M. Cornwall, D. N. Levin, and G. Tiktopoulos, *Phys. Rev. D* **10**, 1145 (1974), [Erratum: *Phys.Rev.D* **11**, 972 (1975)].
- [37] B. W. Lee, C. Quigg, and H. B. Thacker, *Phys. Rev. D* **16**, 1519 (1977).
- [38] C. E. Vayonakis, *Lett. Nuovo Cim.* **17**, 383 (1976).
- [39] M. S. Chanowitz and M. K. Gaillard, *Nucl. Phys. B* **261**, 379 (1985).
- [40] H. G. J. Veltman, *Phys. Rev. D* **41**, 2294 (1990).
- [41] A. Papaefstathiou, T. Robens, and G. Tetlalmatzi-Xolocotzi, *JHEP* **05**, 193 (2021), arXiv:2101.00037 [hep-ph].
- [42] A. Papaefstathiou and G. Tetlalmatzi-Xolocotzi, (2025), arXiv:2501.14866 [hep-ph].
- [43] G. Aad *et al.* (ATLAS), *Eur. Phys. J. C* **80**, 1165 (2020), arXiv:2004.14636 [hep-ex].
- [44] A. M. Sirunyan *et al.* (CMS), *Phys. Lett. B* **798**, 134952 (2019), arXiv:1906.00057 [hep-ex].
- [45] C.-Y. Chen, S. Dawson, and E. Furlan, *Phys. Rev. D* **96**, 015006 (2017), arXiv:1703.06134 [hep-ph].
- [46] M. Carena, H. E. Haber, I. Low, N. R. Shah, and

- C. E. M. Wagner, *Phys. Rev. D* **93**, 035013 (2016), [arXiv:1510.09137 \[hep-ph\]](#).
- [47] D. de Florian *et al.* (LHC Higgs Cross Section Working Group), *CERN Yellow Rep. Monogr.* **2**, 1 (2017), [arXiv:1610.07922 \[hep-ph\]](#).
- [48] J. Alwall, R. Frederix, S. Frixione, V. Hirschi, F. Maltoni, O. Mattelaer, H. S. Shao, T. Stelzer, P. Torrielli, and M. Zaro, *JHEP* **07**, 079 (2014), [arXiv:1405.0301 \[hep-ph\]](#).
- [49] J. M. Butterworth, A. R. Davison, M. Rubin, and G. P. Salam, in *34th International Conference on High Energy Physics* (2008) [arXiv:0810.0409 \[hep-ph\]](#).
- [50] A. J. Larkoski, I. Moulton, and B. Nachman, *Phys. Rept.* **841**, 1 (2020), [arXiv:1709.04464 \[hep-ph\]](#).
- [51] A. Radovic, M. Williams, D. Rousseau, M. Kagan, D. Bonacorsi, A. Himmel, A. Aurisano, K. Terao, and T. Wongjirad, *Nature* **560**, 41 (2018).
- [52] P. Li, Z. Liu, and L.-T. Wang, (2026), [arXiv:2604.14284 \[hep-ph\]](#).
- [53] A. Hayrapetyan *et al.* (CMS), *Phys. Rev. D* **110**, 072012 (2024), [arXiv:2405.05071 \[hep-ex\]](#).
- [54] G. Aad *et al.* (ATLAS), *JHEP* **05**, 075 (2025), [arXiv:2411.07143 \[hep-ex\]](#).
- [55] R. Benbrik, M. Boukidi, M. Ech-chaouy, S. Moretti, K. Salime, and Q.-S. Yan, *JHEP* **03**, 020 (2025), [arXiv:2412.01761 \[hep-ph\]](#).
- [56] C. Oropenza Barrera (CMS), *PoS LHCP2024*, 011 (2025).